DNS analysis of boundary layer flashback in turbulent flow with wall-normal pressure gradient

J.R. Bailey[a,*], E.S. Richardson[a]

[a]*Faculty of Engineering and Physical Sciences, University of Southampton, Southampton SO17 1BJ, UK*

Abstract

The presence of swirl in combustion systems produces a marked change in their boundary layer flashback behaviour. Two aspects of swirling flow are investigated in this study: the effect of the swirl-generated wall-normal pressure gradient, and the effect of misalignment between the mean flow direction and the direction of flame propagation. The analysis employs Direct Numerical Simulation (DNS) of fuel-lean premixed hydrogen-air flames in turbulent planar channel flow with friction Reynolds number of 180. The effect of swirl on the flashback process is investigated by imposing a wall-normal pressure gradient profile. Analysis of the DNS data shows how the resulting differences in flow field and flame topology contribute to the differences in the overall flashback speed. Misalignment of the flow and propagation directions leads to asymmetry in the flame shape statistics as streaks of high velocity fluid in the boundary layer cleave into the flame front at an angle, yielding an increase in flame surface density away from the wall. Swirl has a stabilising effect on the turbulent flame front during flashback along the centre-body

*Corresponding author:
Email address: j.r.bailey@soton.ac.uk (J.R. Bailey)

of a swirling annular flow due to the density stratification across the flame front, and produces a reduction in turbulent consumption speed. However the swirl also sets up a hydrostatic pressure difference that drives the flame forward, and the net effect is that the flashback speed is increased. The dominance of hydrostatic effects motivates development of relatively simple modelling for the effect of swirl on flashback speed. A model accounting for the inviscid momentum balance and for confinement effects is presented which adequately describes the effect of swirl on flashback speed observed in previous experimental studies.
Keywords:
Turbulent channel flow, Turbulent premixed flame, Boundary-layer flashback, Swirl flames, Flashback-limit model

1. Introduction

Industrial Gas Turbines (IGTs) play an important role in power generation. They are able to follow changes in demand, and they have high efficiency, low cost and low NOx emissions. This performance has been achieved using lean premixed combustion, and overwhelmingly with natural gas as the fuel source. However, lowering the carbon intensity of IGTs will require the use of alternative fuels, such as those rich in hydrogen, and new combustion technology, such as fuel-flexible burners that can utilise different and varying fuel sources [1].

Alternative fuels may present opportunities for efficiency and emissions improvements but also challenges. The higher flame speed of hydrogen-rich fuels reduces the risk of lean blow-off but increases the risk of flashback, where

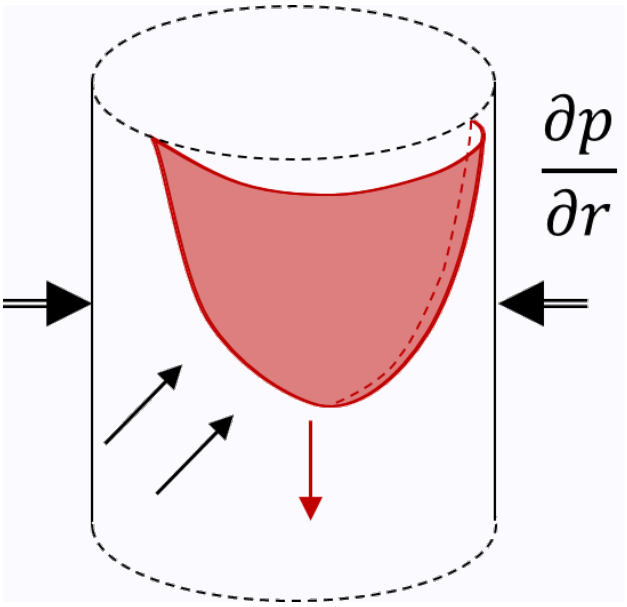

Figure 1: Schematic diagram illustrating boundary-layer flashback along the centre-body of a mixing tube in a swirling flow with radial pressure gradient ($\partial p/\partial r$).

the flame is able to propagate upstream into the premixing section of the IGT. This results in plant shutdowns, damage to equipment, and is a major safety concern. Flashback can occur through a variety of different mechanisms and this work considers boundary-layer flashback where the flame propagates upstream through the lower-velocity boundary layer fluid [1].

Swirling flows are commonly used for fuel mixing and flame stabilisation in IGTs and the effect of swirl on the likelihood of flashback is therefore of critical importance. Experimental investigations of boundary layer flashback in swirling annular flows [2–6] have looked at the flame and flow structures for hydrogen-air and methane-air blends. An increase in swirl was shown to initiate flashback from a previously stable state [2]. A single flame tongue propagates upstream along the boundary layer of the centre-body of the

annular duct while precessing around the centre-body. The flame tongue has a side which leads flame propagation and a trailing side which is facing the oncoming flow [6] as illustrated schematically in Fig. 1. This means that there is a misalignment between the oncoming mean flow and mean flame propagation direction.

Recent experimental [7] and Direct Numerical Simulation (DNS) [8] studies of flashback have investigated non-swirling flows within planar channels where the turbulent flame propagates directly towards the oncoming flow. Here a pressure rise upstream of the flame has been linked to boundary-layer separation and reversed flow ahead of the flame, and increased likelihood and speed of flashback. Boundary layer flashback in swirling flows presents a different variation of pressure through the flame. The pressure rise ahead of the flame front causes flow reversal normal to the flame along the leading side of the flame tongue, but not along the trailing side [3, 6]. The pressure rise ahead of the flame is not linked to boundary-layer separation in swirling flow [6]. These effects result from the misalignment between flow and flame. Swirling flows also show differences in the pressure downstream of the flame front: the centripetal acceleration produces different radial pressure gradients in the higher-density reactants and lower-density products, yielding a further pressure rise across the leading edge of the flame tongue [3, 6, 9]. In non-swirling flows flow acceleration through the flame is associated with a drop in pressure [8].

Models for the prediction of flashback limits have been developed based on boundary-layer separation (without effects of swirl) [10], reproducing flashback limits for hydrogen-air flames at different preheating temperatures in

Table 1: Simulation parameters for the reactive cases

Label	Flow orientation	Fr	$L_x \times L_y \times L_z$	$N_x \times N_y \times N_z$	Re_τ	Da	δ_l/δ	u_τ/S_L
Case 1	Normal (0°)	∞	$5\delta \times 2\delta \times 3\delta$	$600 \times 400 \times 360$	180	0.14	0.09	0.38
Case 2	Oblique (45°)	∞	$5\delta \times 2\delta \times 3\delta$	$600 \times 400 \times 360$	180	0.14	0.09	0.38
Case 3	Normal (0°)	0.07	$7.5\delta \times 2\delta \times 3\delta$	$864 \times 400 \times 360$	180	0.14	0.09	0.38

planar channels and tubes. Modeling for the effects of swirl has been developed considering the inviscid momentum balances for flames within idealised swirl distributions [9], providing predictions of flashback speed and the pressure rise across the flame.

The objective of this study is to investigate how the wall-normal pressure gradient and the misalignment of flow and flashback directions contribute to the different flashback behaviour of swirling and non-swirling flows. The paper proceeds with a description of new DNS data that are used to study these effects. Analysis of the structure of the turbulent flame fronts and of the associated flow fields is then used as a basis for development of an analytical model for the effects of swirl on flashback speed.

2. Formulation

The effects of wall-normal pressure gradient and flow-flame alignment are investigated in DNS of a turbulent planar channel flow. Three cases are

simulated as summarised in Table 1. Case 1 involves a flame that propagates normal to the oncoming flow direction, similar to the configuration studied by Gruber *et al.* [8]. In Case 2 the flow direction is rotated so that it is at an angle of 45° relative to the leading flame edge. Case 3 differs from Case 1 due to the introduction of a wall-normal pressure gradient.

In all cases the channel flow has a friction Reynolds number equal to 180. Premixed hydrogen and air flow along the channel with equivalence ratio of 0.55, temperature of 750 K and a nominal pressure of 1 atm. The laminar flame speed and thickness for a one-dimensional freely-propagating flame at these conditions are $S_L = 7.4$ m.s^{-1} and $\delta_l = 0.52$ mm respectively, resulting in channel-flow Damköhler number based on the laminar flame timescale and unburned wall friction time scale Da= 0.14 as set out in Ref. [11]. The channel walls are non-slip and isothermal, also with a temperature of 750 K. The channel half-height (δ) is 5.76mm and the simulation domain extends 3δ in the periodic z-direction and either 5 or 7.5δ in the inflow/outflow x-direction as specified in Table 1. To give realistic, time-evolving turbulence, the initial velocity field and the inflow velocities during the simulations are obtained from separate auxiliary simulations of fully-developed doubly-periodic turbulent channel flow. These flows are driven by an imposed stream-wise pressure gradient aligned with the x-direction in Cases 1 and 3 (giving a mean flow opposing the direction of mean flame propagation) or oriented 45° from the x-direction for Case 2 (giving a misalignment between flame and flow), as annotated in Figure 2. The auxiliary simulations employ the same grid used by Ref. [8].

Boundary layer flashback in swirling annuli occurs preferentially along

the centre-body of the annulus. Therefore the flame front is initialised asymmetrically as a plane angled with respect to the x-axis. The initial angle of $\pi/5$ radians approximated that seen in laminar, two-dimensional simulations. The composition and temperature fields across the flame are mapped from a one-dimensional flame onto a hyperbolic tangent function with a width of the thermal thickness, as used in Ref. [8]. The temperature of the products is set to transition to the wall temperature along the wall boundary.

Within swirling flows the radial pressure gradient is given by

$$\frac{\partial p}{\partial r} = \rho \frac{V_\theta^2}{r}, \tag{1}$$

where r is the radial distance from the centre of rotation and V_θ the circumferential velocity. In viscous swirling annular flow the circumferential velocity and hence the wall-normal pressure gradient falls to zero at the inner and outer walls of the annulus. In the present planar channel flow simulations, the wall-normal pressure gradient results from the application of a body force acting in y (as annotated for Case 3 in Figure 2) providing y-dependent acceleration g_y. g_y is uniform across the central part of the channel and falls to zero at the walls according to

$$g_y(y) = g\left(1 - \left(1 - \frac{y}{\delta}\right)^4\right). \tag{2}$$

This body force distribution and the value of amplitude $g = 3 \times 10^6 m/s^2$ used for Case 3 correspond approximately to the distribution of circumferential velocity in the low-Reynolds number annular flashback case of Ebi and Clemens [6]. A Froude number is defined using reduced gravity (g') (incorporating the unburned and burned mixture densities, ρ_u and ρ_b):

$$Fr = \frac{S_L}{\sqrt{g'\delta}} \qquad g' = g\left(\frac{\rho_u - \rho_b}{\rho_u}\right), \tag{3}$$

giving a Froude number equal to 0.07 for Case 3. The Froude number is defined characterising the relative importance of flame propagation (S_L) and buoyancy effects ($\sqrt{g\delta}$); this will be used in determining the third relevant velocity scale: the relative velocity between flame and flow ($U_{bulk} - V_f$, where V_f is the lab-frame propagation speed). The relevant flame speed here is the edge-tip displacement speed S_f but to specify this velocity scale a priori and without accepted modelling of its value, the laminar flame speed is used.

The initial pressure field is set equal to 1 atm for Cases 1 and 2. The initial pressure and the target boundary pressures for Case 3 are the hydrostatic values obtained by integrating the product of z-averaged fluid density and g_y, starting from a pressure of 1 atm at the $y = 2\delta$ wall, noting that the density field varies during the simulation.

The flow is simulated with the compressible Navier-Stokes equations and chemical reactions are described by a detailed hydrogen-air combustion mechanism [12] with 9 species and 19 reactions. Thermodynamic properties are polynomial functions of temperature.

The simulation is performed with the three-dimensional DNS code from Sandia, S3D [13]. Spatial differencing uses an eighth-order, explicit, centred, finite-difference scheme with a tenth-order, explicit, spatial filter [14]. A fourth-order, explicit Runge-Kutta scheme [15] is used for time integration. Partially non-reflecting Navier-Stokes characteristic boundary conditions are employed at the inlet and outlet in the x-direction, based on the original formulation [16] and later improvements [17–19].

The simulation employs a Cartesian grid providing 10 grid points within a laminar flame thickness in x and z. In y the 400 grid points give 2 points

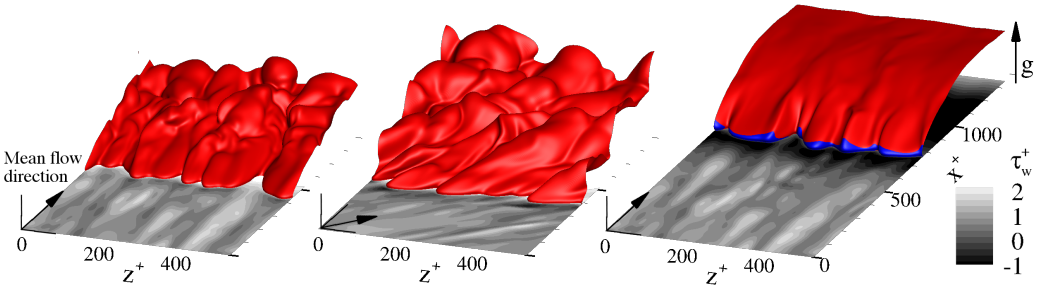

Figure 2: Flame shape ($c = 0.7$ isosurface) after 0.5 ms for Cases 1-3 (left to right), coloured red for positive x-direction velocity and blue for back-flow regions. The shading of the bottom wall shows non-dimensional wall shear stress, τ_w^+. Arrows show the mean flow direction and orientation of the body force g.

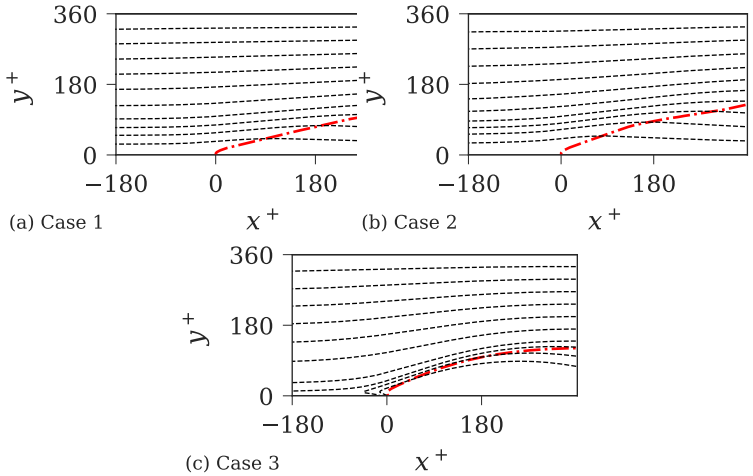

Figure 3: Mean stream surfaces (dashes) and flame position ($\tilde{c} = 0.7$, red dash-dot) in the frame of reference of the flame's leading edge for Cases 1-3 (left to right).

within $1y^+$ and 11 within $10y^+$, for sufficient resolution of the turbulent channel flow [8]. Data sampling begins 0.4 ms after the start of the simulation to allow acoustic perturbations from the initial flow development to exit the

domain. Subsequently, data are recorded for ten wall time units, similar to Ref. [8], sampling every two wall time units. Statistical convergence was checked by comparing the results from each half set of samples.

3. Results and Discussion

3.1. Direct Numerical Simulations

Figure 2 shows the shape of the flame surface for each case, and the presence of high- and low-velocity streaks in the boundary layer. The flames propagate along the boundary layer with the high-velocity streaks cutting the flame into lobes that are aligned with the mean flow direction of the respective cases. Oblique flow (Case 2) produces asymmetrical flame lobes, with the leading side (facing the positive z-direction) longer compared to its trailing side (facing the negative z-direction). In Case 3 the flame surface wrinkling is attenuated away from the wall due to the density change across the flame and strong body force favouring stable density stratification. The flame front is defined by a progress variable isosurface $c = 0.7$, defined in terms of the hydrogen mass fraction.

Figure 3 shows the streamsurfaces of the averaged flow field in the frame of reference of the leading flame edge, averaged over time and the homogeneous z-direction. The $\tilde{c} = 0.7$ iso-surface of Favre-averaged progress variable represents the mean flame location. The fully developed turbulent flow means there is no dependence on the flame's axial channel position. Cases 1 and 2 present similar flow and flame profiles, with an adverse pressure gradient and instantaneously very small regions of negative velocity in the x-direction upstream of the leading points of the flame. For the oblique case (Case 2), flow

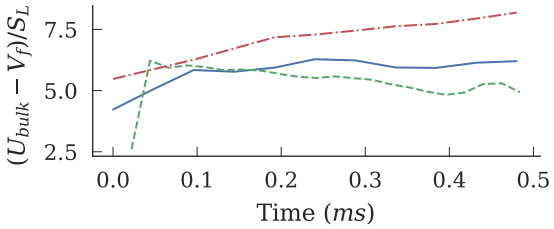

Figure 4: Temporal evolution of relative flashback speed ($U_{bulk} - V_f$). Case 1 - solid blue; Case 2 - green dashed; Case 3 - red dot-dashed.

is reversed in the x-direction and, to a more limited extent, in the streamwise ($x = z$) direction. The wall-normal pressure gradient (Case 3) produces a region of elevated pressure upstream of the flame front, as seen in Refs. [6, 9], that drives a large region of reversed flow that extends downstream through the flame leading edge.

Figure 4 shows the temporal evolution of the flashback speed (lab-frame propagation speed, V_f, relative to the bulk x-direction velocity, $U_{x,bulk}$). After **0.2ms** the flame evolution is weakly time-dependent and the flashback speeds are in the region of 6.2, 4.9 and 8.5 S_L for Cases 1-3 respectively, indicating that misalignment of flow and propagation directions reduces flashback speed, while the body force increases flashback speed.

Figure 5 shows the flame surface density $\overline{|\nabla c|}$ across the flame as a function of the Favre-averaged progress variable on a plane at $5y^+$. This plane was chosen as being representative of the flames' leading points, which are between $2 - 6y^+$ for Cases 1 and 2 and between $5 - 13y^+$ for Case 3. The flame surface density shows slight increases for both the oblique flow and the body force. Increased flame surface density typically increases turbulent

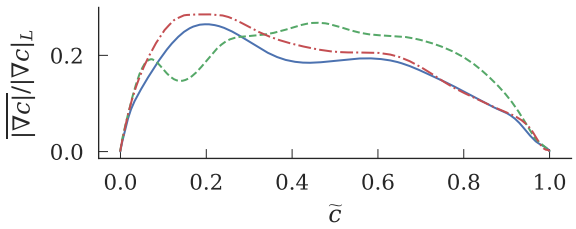

Figure 5: Time- and z-averaged flame surface density relative to laminar flame front versus Favre-averaged progress variable at $5y^+$. Case 1 - solid blue; Case 2 - green dashed; Case 3 - red dot-dashed.

flame speed, but these differences do not explain the differences in flashback speed.

Figure 6 presents the probability density functions of curvature, tangential strain and displacement speed of the $c = 0.7$ isosurface at $5y^+$. Similar trends are observed for the global pdf (over all y^+). The mean curvature and tangential strain rate are both positive for all cases, which is expected to increase the displacement speed for fuel-lean hydrogen flames. Misalignment of the flame propagation with respect to the mean flow direction (Case 2) produces a small reduction in average flame curvature and halves the average tangential strain rate. Conditioning the Case 2 pdfs on the leading and trailing sides of the flame lobes shows that the trailing side sof the flame lobe (the side facing negative z) experience substantially higher tangential strain than the leading side (the side facing positive z). The surface area of the trailing sides is smaller, therefore the overall pdf shape is dominated by the contribution of the leading sides. The pdfs show that the correlation of displacement speed with tangential strain for the $c = 0.7$ isosurface is opposite to the usual trend for fuel-lean hydrogen flames, but we note that this

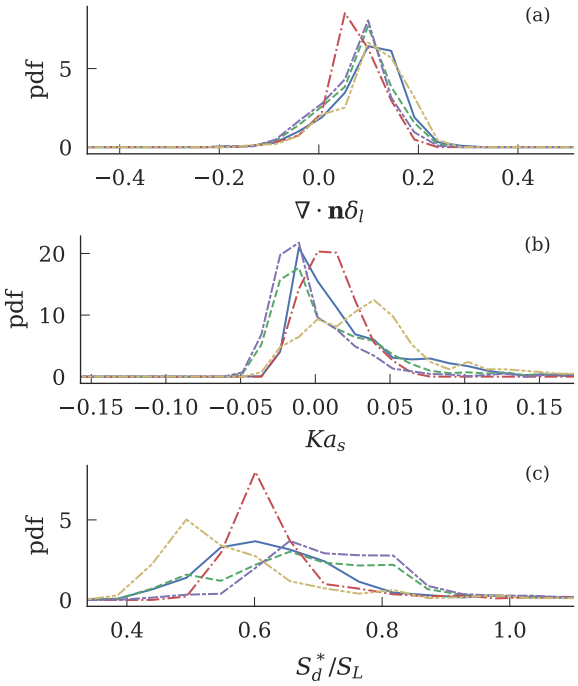

Figure 6: Probability density function (pdf) of normalised curvature ($\nabla \cdot \mathbf{n}\delta_l$), tangential strain ($Ka_s$) and density-weighted displacement speed, S_d^*/S_L, at the flame front (c=0.7) on a plane $y^+ = 5$. Line styles as in Fig. 5, and Case 2 conditioned on leading sides (purple long dash–short dash), Case 2 conditioned on trailing sides (brown dash-dash-dot-dot).

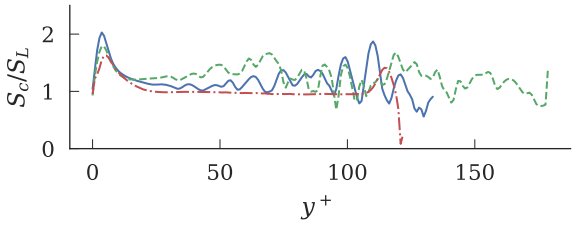

Figure 7: Consumption speed of time- and Favre-averaged reaction rate integrated in y-planes as a function of wall-normal distance (y^+). Line styles as in Fig. 5.

observation is dependent on the proximity to the wall, and hence wall heat transfer and mean curvature at the leading edge of the flame. The results, but not the overall conclusions, are also sensitive to the choice of progress variable and value used to define the flame. However the net effect on the average of displacement speed over the whole flame surface is rather small, increasing from 0.95 S_L in Case 1 to 0.96 S_L in Case 2. The stabilising effect of the wall-normal pressure gradient (Case 3) narrows the distributions of curvature, strain and displacement speed, contributing to a reduction of the overall surface-averaged displacement speed to 0.87 S_L.

Figure 7 shows the turbulent consumption speed calculated from the time- and z-averaged reaction-rate fields as a function of the wall-normal distance. All cases show a peak in turbulent consumption speed at around $2-10y^+$ at the highly-curved leading edge of the flame. The peak turbulent consumption speed is highest for Case 1, although the average consumption speed is higher in Case 2. The wall-normal pressure gradient reduces the turbulent consumption speed for all y^+ for Case 3, consistent with its lower displacement speed, and supression of flame wrinkling away from the wall (at $> 5y^+$).

The flashback speed in Case 3 is higher than Case 1 (Fig. 4) despite its

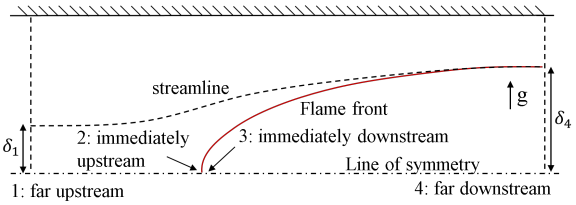

Figure 8: Control volume geometry for modelling of the flashback speed.

lower overall flame surface area (Fig. 2), surface average displacement speed (Fig. 6) and turbulent consumption speed (Fig. 7). Therefore the main reason for the increase in flashback speed in Case 3 is enhancement of the flow reversal at the leading edge of the flame due to the wall-normal pressure gradient (Fig. 3).

3.2. Momentum-Balance Model

A first model for the flashback speed is developed considering the steady-state momentum balance within a control volume moving with the flame, as illustrated in Fig. 8. This is similar to the approach of Ruetsch *et al.* [20] whose model predicts the effect of flame density ratio on edge-flame speed in the absence of body forces. Here Ruetsch's model is extended for application to swirling annular flows by consider the effects of a body force and of flow confinement.

The Ruetsch model is derived considering inviscid, adiabatic flow along a streamline passing through the leading point of the flame, and considering the mass and momentum balance within a control volume defined by a streamsurface exactly enclosing the burned products of the flame at location (4), as in Fig. 8. The density is constant in the unburnt mixture (ρ_u) and constant in the burnt mixture (ρ_b). The flow is locally one-dimensional along

the line of stoichiometry through the leading point of the flame. Together these allow the Rankine-Hugoniot relations to be applied between points (2) and (3), and the conservation of mechanical energy between points (1) and (2), and (3) and (4). The flow velocity is uniform across the flame streamsurface at points (1) and (4) and it was assumed that the pressures at points 1 (P_1) and 4 (P_4), and acting on the streamsurface (P_s) were equal. Ruetsch *et al.* [20] showed that these assumptions determine that the edge flame moves relative to the unburnt mixture at speed

$$u_1 = S_f \sqrt{\frac{\rho_u}{\rho_b}} \tag{4}$$

where S_f is the displacement speed of the leading edge of the flame, taken by Ruetsch *et al.* to be the laminar flame speed, S_L.

Here the model is extended by considering flashback in a constant area duct of height 2δ. Control volume analysis of the DNS Case 3 (not shown) indicates that wall shear stress makes a minor contribution to the pressure-dominated momentum balance in the vicinity of the flame, therefore the flow is again assumed to be inviscid, as well as adiabatic. Away from the wall the flame propagates at a small angle from the wall normal (see Fig. 2) and it is assumed that the flow and flame can be approximated as being parallel to the wall at the control volume exit. These assumptions are equivalent to those of Ruetsch *et al.* [20]. This allows the application of the one-dimensional relations along the four points of the streamline through the leading point of the flame, and a mass and momentum balance over the control volume enclosed by the streamline.

The model is extended to this flashback configuration, accounting for the effect of a body force and flow confinement. To account for the body force,

the pressures P_1, P_4 and P_s are no longer assumed to be equal. Instead a wall-normal pressure gradient is imposed by a uniform body force, g. The pressures P_1, P_4 and P_s and those at the inlet and exit of the control volume now depend on the streamline heights δ_1 and δ_4. These pressures are calculated by integrating from the top wall of the channel, as drawn in Fig. 8, where $P = P_{tw}$. The pressure along the flame streamsurface is assumed to equal the average pressure at the exit of the control volume between δ_1 and δ_4. To account for confinement the pressure P_{tw} is assumed to change along the channel by $\Delta P_{tw} = P_{tw,4} - P_{tw,1}$. This pressure change is calculated by solving the mass and momentum balance in the unburned region between the streamline and the top wall.

The final model takes three independent non-dimensional input variables: confinement ratio δ/δ_4, density ratio ρ_u/ρ_b, and Froude number $S_f/\sqrt{g'\delta_4}$, where g' is given by Eq. 3. This predicts three non-dimensional output variables: height ratio $\delta_1' = \delta_1/\delta_4$, pressure drop $\Delta P_{tw}' = \Delta P_{tw}/(\frac{1}{2}\rho_u u_1^2)$ and velocity ratio $u_1' = u_1/S_f$. These output variables are given by:

$$\delta_1' = \frac{(\rho_u/\rho_b)(Fr^2 u_1'^2 - 1) - \Delta P_{tw}' Fr^2}{(\rho_u/\rho_b)((\rho_u/\rho_b)Fr^2 u_1'^2 + 1/2)} \tag{5}$$

$$u_1'^2 = \frac{(\rho_u/\rho_b) - 1 + \frac{2}{Fr^2}}{1 - (\rho_u/\rho_b)\delta_1'^2 - \Delta P_{tw}'} \tag{6}$$

$$\Delta P_{tw}' = -2\frac{(1-\delta_1')}{(2\delta/\delta_4 - 1)} - \frac{(\delta_1' - 1)^2}{u_1'^2 Fr^2 (2\delta/\delta_4 - \delta_1')} \tag{7}$$

which are solved numerically.

A second simpler model is also considered in order to describe the key dependence of flashback speed on the wall-normal pressure gradient. The model draws an analogy between the pressure-driven flashback process and

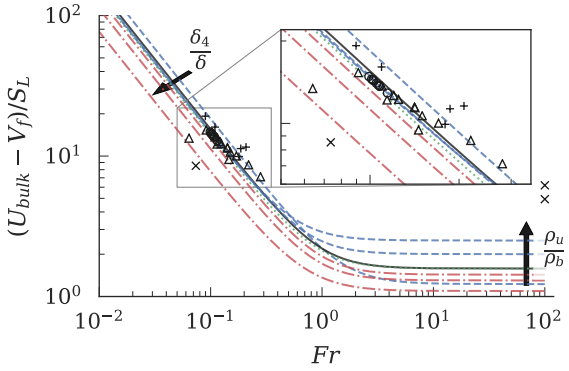

Figure 9: Relative flashback speed as a function of Froude number. From the model: solid black is density ratio (ρ_u/ρ_b) 2.5 and no confinement ($\delta_4/\delta = 0$), blue dashed show density ratios 1.5, 4.0 and 6.0; red dot-dashed are confinement ratios (δ/δ_4) of 4 and 2. The green dotted shows $(u_1/S_f)^2 = (\rho_u/\rho_b) + 2/Fr^2$. Experimental data on swirling, turbulent boundary-layer flashback: + [4–6, 23, 24], ◯ [3], △ [2]. The × are the DNS cases from this paper.

the propagation of a gravity current in density-stratified flow [21, 22], but can also be derived by simplifying the model above. Gravity currents involve a layer of fluid spreading along a surface driven by hydrostatic pressure differences. Theoretical analysis successfully predicts that gravity currents achieve asymptotic velocities approximately $\sqrt{2}$ times their buoyancy velocity when flowing through an infinite expanse of fluid [21]. Here the gravity current velocity estimate is modified by combining it with a deflagrative propagation contribution given by Ruetsch's original model for unconfined edge flames in the absence of body forces:

$$\left(\frac{u_1}{S_f}\right)^2 = \frac{\rho_u}{\rho_b} + \frac{2}{Fr^2}. \tag{8}$$

Figure 9 presents the results of the models compared to experimental measurements of flashback in swirling annular flows. The results of the first

model for different density and confinement ratios are shown. Experimental data is shown for swirling flows (+ [4–6, 23, 24], ◯ [3], △ [2]). The + represent data for flashback speeds while ◯ and △ are flashback limits.

The results from the models show a transition from high Fr where the body force has little influence and the original Ruetsch model is recovered, to low Fr where the body force is dominant. The density ratio, ρ_u/ρ_b, influences propagation speed at high Fr where $(U_{bulk} - V_f)/S_L = (\rho_u/\rho_b)^{1/2}$, but has little influence at low Fr. The model shows confinement having a consistent influence across the range of Fr.

The models provide encouraging prediction of the trend seen in the experimental data for flashback in swirling flows in Refs. [2–6, 23]. The gravity current model appears to describe the key process driving the boundary layer flashback process in swirling flow, despite its extreme simplicity.

4. Conclusion

Boundary layer flashback speed is increased significantly by wall-normal pressure gradients that can be generated by swirl. The pressure gradient at the centre-body of a swirling annular flow acts to attenuate wrinkling of the flame. In the DNS Case investigated here, the wall-normal pressure gradient also led to reduced surface-averaged displacement speed and turbulent consumption speed. The increase in flashback speed is therefore attributed to a region of reverse flow around the leading edge of the flame that is driven by stream-wise hydrostatic pressure differences generated by the wall-normal pressure gradient. The dominance of hydrostatic effects motivates development of relatively simple modelling for the effect of swirl on flashback speed.

A model accounting for the inviscid momentum balance and for confinement effects is presented which adequately describes the effect of swirl on flashback speed observed in previous experimental studies. The misalignment of flashback direction and flow direction that is anticipated in swirling flows also contributes to changes in flame structure: streaks of high velocity fluid in the boundary layer cleave into the flame front at an angle, producing asymmetric flame strain and curvature distributions and yielding an increase in flame surface density away from the wall, however the effects of flow alignment on flame topology do not alter the flashback speed significantly in the case investigated.

Acknowledgments

We acknowledge financial support from the EPSRC (EP/L015382/1, EP/K024876/1) and use of ARCHER UK National Supercomputing Service (http://www.archer.ac.uk) and the IRIDIS High Performance Computing Facility at the University of Southampton. Archival data for this paper are available at (doi:to be provided upon acceptance).

References

[1] S. Taamallah, K. Vogiatzaki, F. M. Alzahrani, E. M. A. Mokheimer, M. A. Habib, A. F. Ghoniem, Fuel flexibility, stability and emissions in premixed hydrogen-rich gas turbine combustion: Technology, fundamentals, and numerical simulations, Appl. Energy 154 (2015) 1020–1047.

[2] A. Nauert, P. Petersson, M. Linne, A. Dreizler, Experimental analysis of

flashback in lean premixed swirling flames: Conditions close to flashback, Exp. Fluids 43 (2007) 89–100.

[3] C. Heeger, R. L. Gordon, M. J. Tummers, T. Sattelmayer, A. Dreizler, Experimental analysis of flashback in lean premixed swirling flames: Upstream flame propagation, Exp. Fluids 49 (2010) 853–863.

[4] D. Ebi, N. T. Clemens, in: 17th Int. Symp. Appl. Laser Tech. to Fluid Mech., Lisbon, Portugal, 2014.

[5] D. Ebi, N. T. Clemens, Flow-flame interaction in turbulent boundary layer flashback of swirl flames, Proc. 9th Int. Symp. Turbul. Shear Flow Phenom. (2015).

[6] D. Ebi, N. T. Clemens, Experimental investigation of upstream flame propagation during boundary layer flashback of swirl flames, Combust. Flame 168 (2016) 39–52.

[7] C. Eichler, T. Sattelmayer, Premixed flame flashback in wall boundary layers studied by long-distance micro-PIV, Exp. Fluids 52 (2012) 347–360.

[8] A. Gruber, J. H. Chen, D. Valiev, C. K. Law, Direct numerical simulation of premixed flame boundary layer flashback in turbulent channel flow, J. Fluid Mech. 709 (2012) 516–542.

[9] N. Karimi, C. Heeger, L. Christodoulou, A. Dreizler, Experimental and theoretical investigation of the flashback of a swirling, bluff-body stabilised, premixed flame, Zeitschrift fur Phys. Chemie 229 (2015) 663–689.

[10] V. Hoferichter, C. Hirsch, T. Sattelmayer, Prediction of Confined Flame Flashback Limits Using Boundary Layer Separation Theory, J. Eng. Gas Turbines Power 139 (2016) 021505 1–10.

[11] A. Gruber, R. Sankaran, E. R. Hawkes, J. H. Chen, Turbulent flame-wall interaction: a direct numerical simulation study, J. Fluid Mech. 658 (2010) 5–32.

[12] J. Li, Z. Zhao, A. Kazakov, F. L. Dryer, An updated comprehensive kinetic model of hydrogen combustion, Int. J. Chem. Kinet. 36 (2004) 566–575.

[13] J. H. Chen, A. Choudhary, B. De Supinski, M. Devries, E. R. Hawkes, S. Klasky, W. K. Liao, K. L. Ma, J. Mellor-Crummey, N. Podhorszki, R. Sankaran, S. Shende, C. S. Yoo, Terascale direct numerical simulations of turbulent combustion using S3D, Comput. Sci. Discov. 2 (2009) 015001.

[14] C. A. Kennedy, M. H. Carpenter, Several new numerical methods for compressible shear-layer simulations, Appl. Numer. Math. 14 (1994) 397–433.

[15] C. A. Kennedy, M. H. Carpenter, R. M. Lewis, Low-storage, explicit Runge-Kutta schemes for the compressible Navier-Stokes equations, Appl. Numer. Math. 35 (2000) 177–219.

[16] T. J. Poinsot, S. K. Lele, Boundary conditions for direct simulations of compressible viscous flows, J. Comput. Phys. 101 (1992) 104–129.

[17] J. C. Sutherland, C. A. Kennedy, Improved boundary conditions for viscous, reacting, compressible flows, J. Comput. Phys. 191 (2003) 502–524.

[18] C. S. Yoo, Y. Wang, A. Trouvé, H. G. Im, Characteristic boundary conditions for direct simulations of turbulent counterflow flames, Combust. Theory Model. 9 (2005) 617–646.

[19] C. S. Yoo, H. G. Im, Characteristic boundary conditions for simulations of compressible reacting flows with multi-dimensional, viscous and reaction effects, Combust. Theory Model. 11 (2007) 259–286.

[20] G. R. Ruetsch, L. Vervisch, A. Liñán, Effects of heat release on triple flames, Phys. Fluids 7 (1995) 1447–1454.

[21] T. B. Benjamin, Gravity currents and related phenomena, Journal of Fluid Mechanics 31 (1968) 209–248.

[22] C. Härtel, E. Meiburg, F. Necker, Analysis and direct numerical simulation of the flow at a gravity-current head. Part 1. Flow topology and front speed for slip and no-slip boundaries, J. Fluid Mech. 418 (2000) 189–212.

[23] D. Ebi, R. Ranjan, N. T. Clemens, Coupling between premixed flame propagation and swirl flow during boundary layer flashback, Exp. Fluids 59 (2018) 109.

[24] R. Ranjan, D. F. Ebi, N. T. Clemens, Role of inertial forces in flame-flow interaction during premixed swirl flame flashback, Proc. Combust. Inst. 37 (2019) 5155–5162.